



**HAL**  
open science

# Kinetics of the Electronic States of Molecular Nitrogen in a Recombining Air/Argon Plasma

Ulysse Dubuet, Pierre Mariotto, Marie-Yvonne Perrin, Christophe O Laux

► **To cite this version:**

Ulysse Dubuet, Pierre Mariotto, Marie-Yvonne Perrin, Christophe O Laux. Kinetics of the Electronic States of Molecular Nitrogen in a Recombining Air/Argon Plasma. AIAA SCITECH 2022 Forum, American Institute of Aeronautics and Astronautics, Jan 2022, San Diego, CA (en ligne), United States. 10.2514/6.2022-1637 . hal-03579548

**HAL Id: hal-03579548**

**<https://hal.science/hal-03579548>**

Submitted on 18 Feb 2022

**HAL** is a multi-disciplinary open access archive for the deposit and dissemination of scientific research documents, whether they are published or not. The documents may come from teaching and research institutions in France or abroad, or from public or private research centers.

L'archive ouverte pluridisciplinaire **HAL**, est destinée au dépôt et à la diffusion de documents scientifiques de niveau recherche, publiés ou non, émanant des établissements d'enseignement et de recherche français ou étrangers, des laboratoires publics ou privés.

# Kinetics of the Electronic States of Molecular Nitrogen in a Recombining Air/Argon Plasma

Ulysse Dubuet\*, Pierre Mariotto†,  
Marie-Yvonne Perrin‡ and Christophe O. Laux§

*Laboratoire EM2C, CNRS UPR 288, CentraleSupélec, Université Paris-Saclay, 3 rue Joliot-Curie, Gif-sur-Yvette, France*

**An electronic-specific collisional-radiative (CR) model of molecular nitrogen ( $N_2$ ) is presented and applied to the study of a recombining air plasma. This plasma is produced at local thermodynamic equilibrium at 8000 K and 1 atm by a 50-kW Inductively Coupled Plasma torch and passes through a water-cooled tube that forces rapid cooling and recombination. The electronic state-specific model takes into account many processes, including (but not limited to) predissociation of  $N_2(C)$ , collisional quenching, and radiation. The 0D simulations are compared with measurements of the nonequilibrium species densities.**

## I. Introduction

**D**uring atmospheric entry, a spacecraft receives a significant radiative heat flux from the shock layer that forms in front of the capsule. Designing the Thermal Protection System (TPS) requires determining the heat flux on the vehicle accurately. While the prediction of the radiative heat flux to the forebody has been thoroughly investigated, the prediction of radiation on the afterbody still suffers from large uncertainties [1]. Indeed, the recombination kinetics in the afterbody region are complex and lead to non-Boltzmann population distributions of the strongest radiative species.

Experiments have been performed to obtain data representative of such recombination conditions [2–6]. To this end, an Inductively Coupled Plasma (ICP) torch was used to heat an air/argon mixture to equilibrium conditions at 8000 K and 1 atm. The gas was then forced to cool while flowing through a water-cooled tube rapidly. Optical Emission Spectroscopy (OES) diagnostics were applied to know the nonequilibrium state of the gas at the outlet of tubes of lengths ranging from 10 to 65 cm. These measurements are useful to assess state-of-the-art kinetic models.

Air-argon mixture experiments were performed at Stanford University by Gessman *et al.* [2,3]. At the inlet of the tube (outlet of the ICP torch), the air-argon mixture is in Local Thermodynamic Equilibrium (LTE) at 8000 K and atmospheric pressure. The water-cooled tube then cools the plasma to 2500 K in approximately 2 ms. The decrease of temperature from 8000 K to 2500 K is fast enough for the gas to depart from chemical and Boltzmann equilibrium at the outlet of the tube. NO and  $N_2$  excited electronic states were found to be strong emitters of the recombining plasma, and their number densities were measured by OES.

In our previous work [7], we developed an electronic state-specific model for NO and we simulated the kinetics along the centerline of the water cooled tube [2,3]. The model was able to predict the nonequilibrium densities of electrons and several NO excited electronic states. In the present study, we extend the model by including  $N_2$  excited electronic states. Then we update our simulations and we compare the predictions of  $N_2(C^3\Pi_u)$ , NO( $A^2\Sigma^+$ ), NO( $B^2\Pi$ ), NO( $C^2\Pi$ ), NO( $D^2\Sigma^+$ ) and electron densities with measurements along the water-cooled tube.

---

\* Ph.D. Candidate, Laboratoire EM2C, CNRS UPR288, CentraleSupélec, Université Paris-Saclay, AIAA Member.

† Ph.D. Candidate, Laboratoire EM2C, CNRS UPR288, CentraleSupélec, Université Paris-Saclay.

‡ Senior Research Scientist, Laboratoire EM2C, CNRS UPR288, CentraleSupélec, Université Paris-Saclay.

§ Professor, Laboratoire EM2C, CNRS UPR288, CentraleSupélec, Université Paris-Saclay, AIAA Fellow.

## II. Experimental setup

The experimental setup is thoroughly described in [2]. A dissociated high-temperature plasma is forced to recombine by rapid cooling. The equilibrium air/argon plasma is generated using a 50-kW ICP plasma torch facility. The plasma then flows through a water-cooled tube (diameter 1 cm, length ranging from 10 to 65 cm) to impose fast cooling (see Figure 1).

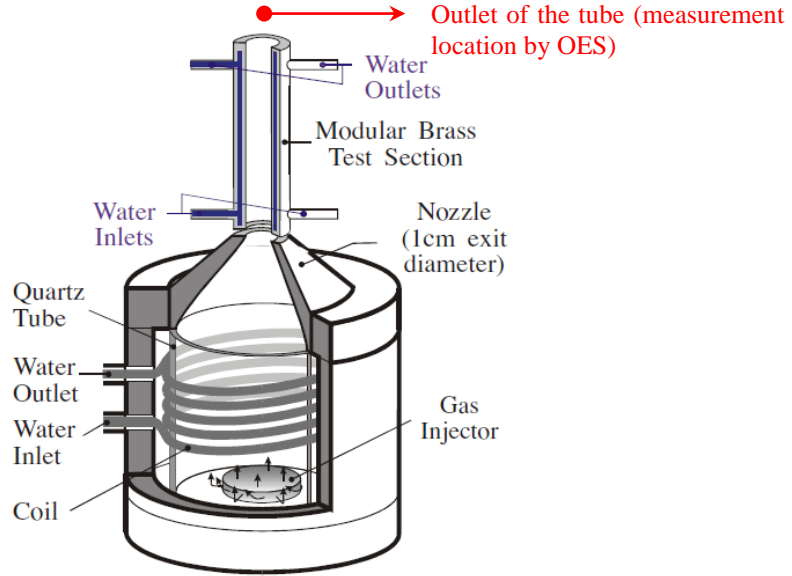


**Figure 1 Schematic of the water-cooled tube (at the top) and plasma torch.**

The flow rates at the entrance of the torch are 15.6 slpm of air, 162 slpm of argon, and 2.3 slpm of  $H_2$ . At the inlet of the tube (outlet of the torch), the gas is in thermal and chemical equilibrium at approximately 8000 K. At the exit of the 65-cm tube, the temperature is approximately 2500 K. Emission spectroscopy was performed at the tube outlet (see Figure 1) for different tube lengths: 0, 10, 15, 40, 50 and 65 cm. The temperatures were measured using atomic lines of oxygen (777.3 nm), nitrogen (746.8 nm), argon (763.5 nm), and hydrogen ( $H_\alpha$ ,  $H_\beta$ ) for tube lengths of 0, 10, and 15 cm; and OH A-X emission bands around 308 nm for longer tube lengths (40, 50 and 65 cm). The electron densities were obtained using the Stark broadening of the  $H_\beta$  line for 0, 10, and 15 cm long tubes. In Ref. [2], for longer tube lengths (40, 50, and 65 cm), the electron number density was obtained assuming partial equilibrium between the electrons and  $NO(C^2\Pi)$  and thus using  $NO(C^2\Pi)$  absolute density measurements.

Overpopulation factors are defined in Eq. (1) as the ratio between the density of species M and its equilibrium density:

$$\rho_M = \frac{[M]}{[M]_{eq}} \quad (1)$$

The overpopulation factors of the  $N_2 C^3\Pi_u$  state were measured by Gessman *et al.* [2] using OES between 320 and 400 nm and are given in Table 1 for different tube lengths. We also reproduce the measured temperatures at the corresponding tube lengths in this Table. The departure from equilibrium is very significant for tube lengths longer than 40 cm, with  $N_2(C)$  overpopulation factors ranging between  $10^5$  and  $10^{11}$ .

**Table 1  $N_2(C)$  overpopulation factor and temperatures at different lengths of the tube.**

z [cm]	0	10	15	40	50	65
T [K]	7980±144	6687±144	5863±125	3450±150	2800±100	2510±100
$N_2(C^3\Pi_u)$	1	1	1	$2.5 \cdot 10^5$	$7 \cdot 10^8$	$3.5 \cdot 10^{11}$

### III. Kinetic model and simulation parameters

This kinetic model is an extension of the model presented in [7]. We added the excited electronic levels of  $N_2$  ( $X^1\Sigma_g^+$ ,  $A^3\Sigma_u^+$ ,  $A'^5\Sigma_g^+$ ,  $B^3\Pi_g$ ,  $B'^3\Sigma_u$ ,  $C^3\Pi_u$ ,  $W^3\Delta_u$ ,  $a'^1\Sigma_u^-$ ,  $a^1\Pi_g$ ,  $b^1\Pi_u$ ,  $b'^1\Sigma_u^+$ ,  $c^1\Pi_u$ ,  $c'^1\Sigma_u^+$ ,  $o'^1\Pi_u$ ) and the collisional/radiative processes between them. We assume that the rovibrational levels within the electronic levels follow Boltzmann distributions at the gas temperature  $T_g$ . We compute the electronic state-specific rate constants of reactions including only  $N$ ,  $N_2$ ,  $Ar$ ,  $N^+$ ,  $N_2^+$ ,  $Ar^+$ , and electrons as follows: first, we assume that  $T_g=T_{vib}=T_{rot}$ ; secondly, we compute all vibrationally specific rate constants with the  $N_2$  CR model developed by Laux *et al.* [8] and updated by Mariotto [9]; thirdly we average the vibrationally specific coefficients into electronically specific coefficients by applying the Weighted Rate Coefficient (WRC) method described in [10]. The model includes reactions of excitation, ionization and dissociation by electron and heavy-particles impact, the ternary recombination into  $N_2$  excited states by heavy-particle impact, the predissociation (and inverse predissociation) of  $N_2(B^3\Pi_g)$  and  $N_2(C^3\Pi_u)$  states, and the heavy-particle impact excitation and deexcitation processes such as intersystem collisional transfer of excitation (ICT), non-resonant collisional quenching and energy pooling.

For the other reactions, we use rate constants taken from the literature [11–15]. The radiative lifetimes of  $N_2(B^3\Pi_g)$  and  $N_2(C^3\Pi_u)$  states are obtained by applying the WRC method (Boltzmann vibrational distribution at  $T_{vib}=T_g$ ) with the vibrational lifetimes of Laux [16].

The 0D-simulations are performed along the centerline of the recombination tube. More details on the simulation conditions can be found in [7].

### IV. Results and discussion

The kinetic simulations along the tube axis offer some insights into the main species evolution and the dominant populating and depleting processes. Figure 2 compares the global species mole fractions obtained with the present model and the equilibrium densities along the tube axis. The equilibrium densities are calculated at the gas temperatures measured at each axial location and at 1 atm using NASA CEA code [17]. Colored bands represent the uncertainties.

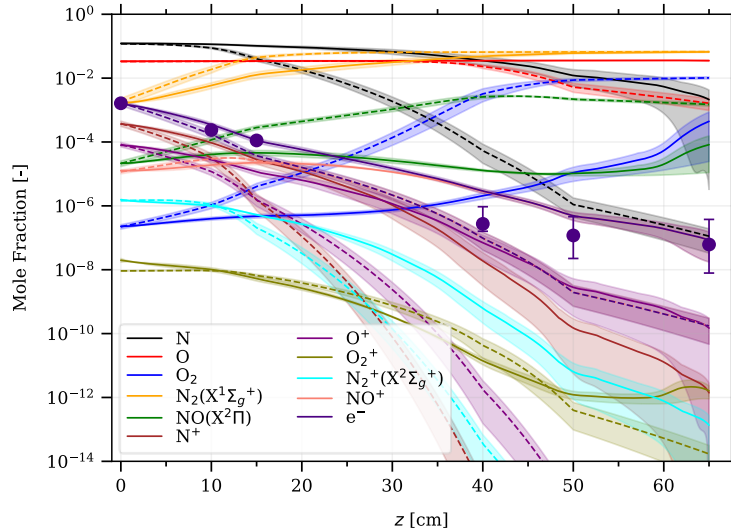


**Figure 2 Species mole fractions along the tube axis. Solid lines correspond to the predictions of the present kinetic model. Dashed lines correspond to chemical equilibrium densities. The measured electron mole fraction [2,3] is also shown for comparison purposes (purple points).**

We observe strong nonequilibrium for the  $N$  and  $O$  atoms. Oxygen recombination is frozen in the tube, and the oxygen atoms depart from chemical equilibrium after 40 cm, with an overpopulation factor  $\rho(O)$  up to 21 at 65 cm. The density of  $N$  decreases by a factor of 80 between 0 and 65 cm. Its departure from equilibrium starts at 10 cm.

After 40 cm, its overpopulation factor  $\rho(N)$  exceeds 650 and reaches  $\sim 14 \times 10^3$  at 65 cm. The nonequilibrium populations of these atoms are the root cause for the nonequilibrium populations of NO and  $N_2$  excited states, and for the nonequilibrium populations of ions and electrons.

We also observe that the electron population is equal to the population of ions  $NO^+$ , as seen with the previous model [2,3]. The electron number densities were also measured at different positions along the tube axis [2,3]. Figure 3 compares the measurements to the simulations. The model slightly overpredicts the electron density along the tube axis, especially at 40 cm, where the discrepancy approximately reaches a factor of 10. At 50 cm, the model agrees with the experiment within the error bars, but there is still a factor of 4 between the simulated and measured electron mole fractions. At 65 cm, the model and the measurements agree well.

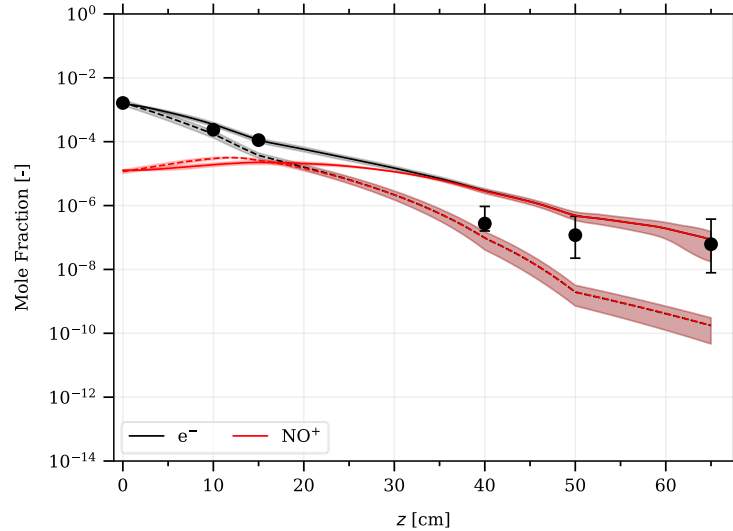


**Figure 3 Electron (black) and  $NO^+$  (red) mole fraction along the tube axis: simulations using the current model (solid lines), measurements [2,3] (black dots – for electron mole fractions only) and chemical equilibrium (dashed lines).**

The populations of the excited electronic states of nitric oxide have also been simulated with the current model. We compare on Figure 4, Figure 5, Figure 6, and Figure 7 the mole fractions of NO A, B, C, and D electronic states obtained using the current model to the measurements made by Gessman [2,3] and to the equilibrium mole fractions.

The new model gives approximately the same results as the previous one [7], and the conclusions are the same. NO(C) population is driven by inverse predissociation of N and O atoms. It is also in partial equilibrium with NO(D) through collisional quenching reactions, both levels being close in energy. They are the main cause for NO(A) overpopulation through spontaneous emission, even though the electronic energy transfer with  $N_2(A)$  also plays an important role in NO(A) population. The excited levels are depleted mostly by collisional quenching (with  $N_2$  and argon).

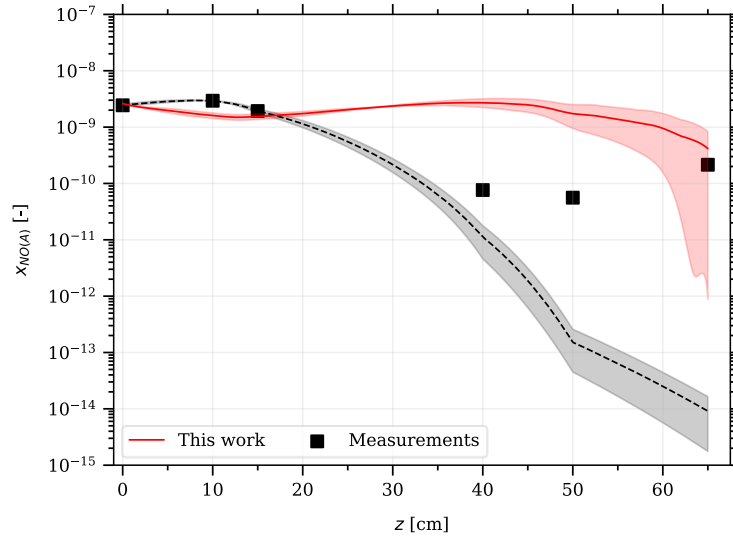


Figure 4 Mole fraction of NO(A<sup>2</sup>Σ<sup>+</sup>): simulations using the current model (red line), measurements [2,3] (black squares), and equilibrium (black line).

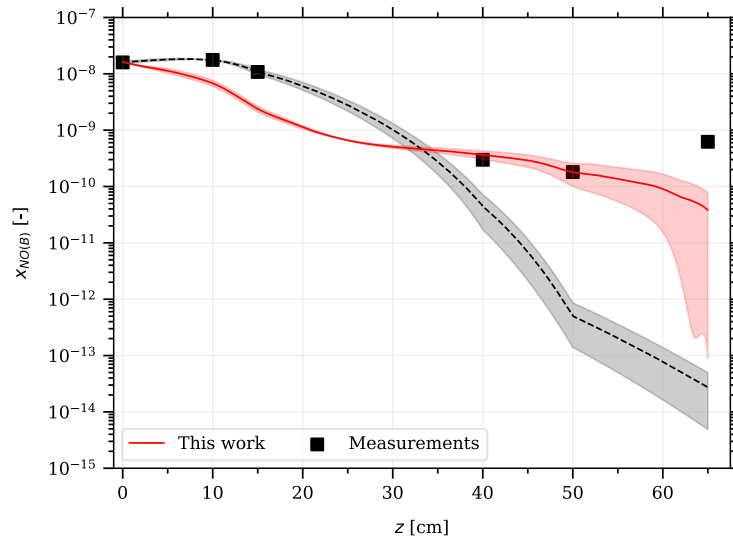
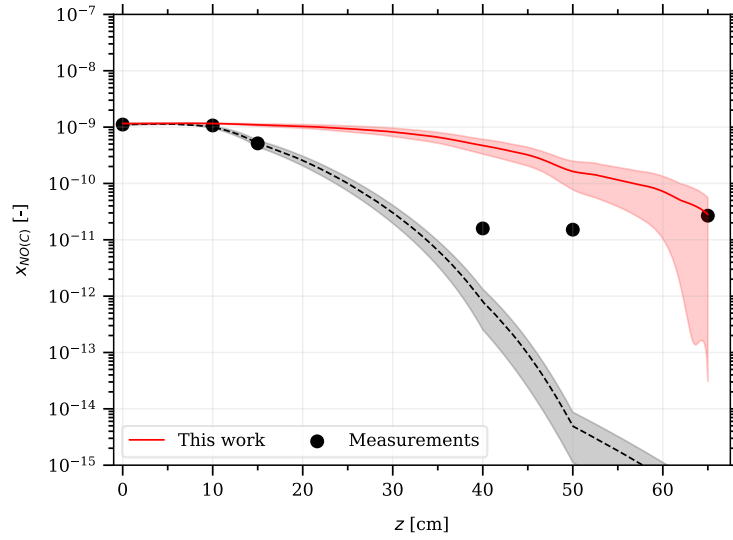
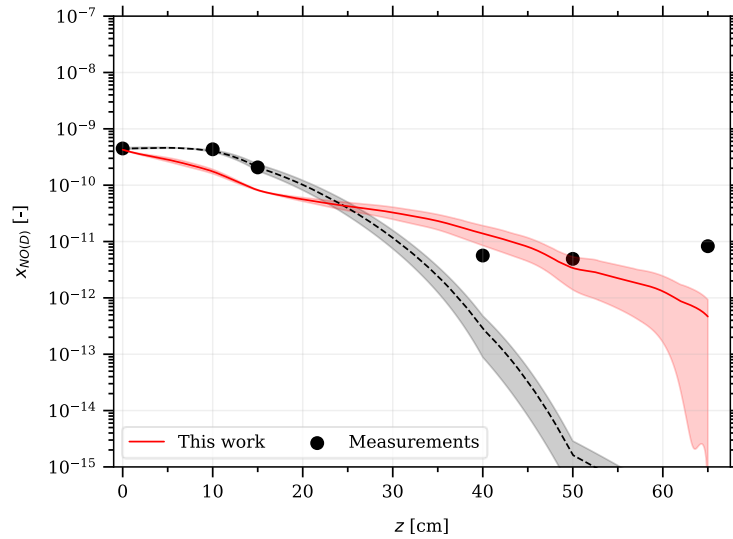


Figure 5 Mole fraction of NO(B<sup>2</sup>Π): simulations using the current model (red line), measurements [2,3] (black squares), and equilibrium (dashed black line).



**Figure 6 Mole fraction of  $\text{NO}(\text{C}^2\Pi)$ : simulations using the current model (red line), measurements [2,3] (black dots), and equilibrium (dashed black line).**



**Figure 7 Mole fraction of  $\text{NO}(\text{D}^2\Sigma^+)$ : simulations using the current model (red line), measurements [2,3] (black dots), and equilibrium (dashed black line).**

Finally, we compare in Figure 8 the simulated mole fraction of  $\text{N}_2(\text{C}^3\Pi_u)$  to the measurements made by Gessman [2,3]. There are important discrepancies. While the model overpredicts  $\text{N}_2(\text{C}^3\Pi_u)$  population before 40 cm (by a factor 1.7 at 10 cm, 6.6 at 15 cm, and 2.6 at 40 cm), the density of the excited state then decreases by several orders of magnitude. The population is largely underpredicted for tube lengths above 50, by a factor of 4 at 50 cm and by 3 orders of magnitude at 65 cm.

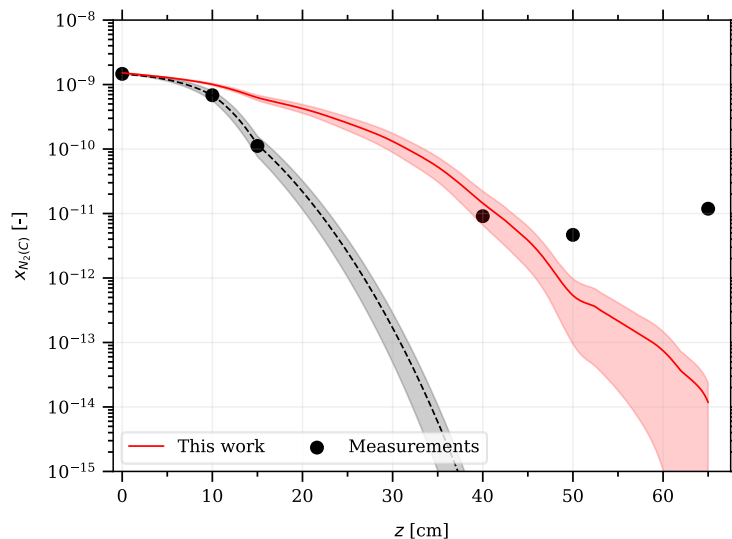


**Figure 8 Mole fraction of  $N_2(C^3\Pi_u)$ : simulations using the current model (red line), measurements [2,3] (black dots), and equilibrium (dashed black line).**

With the current model and considering the *net* reaction rates ( $dn = dn_{\text{forward}} - dn_{\text{reverse}}$ ),  $N_2(C^3\Pi_u)$  is mainly produced through inverse predissociation, and consumed by radiation and collisional quenching into  $N_2(B^3\Pi_g)$  (the transition being optically allowed) by impact with  $N_2(X^1\Sigma_g^+)$ .

The important discrepancies at larger tube lengths may suggest that we are missing some important processes, or that our electronic-specific description of  $N_2$  is too coarse. For instance, in the short-lived afterglow [18], a vibrationally specific model of  $N_2$  is needed to capture the increase of  $N_2(A^3\Sigma_u^+)$  densities after a first drop. This increase can indeed be explained by V-V pumping-up mechanisms followed by V-E transfers. The increase of density in the short-lived afterglow looks like the increases of density observed at the exit of the 65-cm water-cooled tube. It may be interesting to explore this lead by using a vibrationally specific model for  $N_2$ .

## V. Conclusions

We presented an electronic state-specific kinetic model for air. We completed our previous nitric oxide CR model [7] with a nitrogen CR model [9]. The latter model was vibrationally specific; thus, we averaged its coefficients into electronic state-specific constants using the Weighted-Rate Coefficient (WRC) method.

We assessed this new model by comparison to a water-cooled tube experiment [2,3]. In this experiment, the cooling of the air mixture is so fast that the gas departs from chemical and Boltzmann equilibrium. We performed 0D kinetic simulation along the tube axis. We compared the densities of key species predicted by the model to measurements. First, we observe that including the  $N_2$  CR model in the NO CR model does not change the predictions regarding the densities of electrons and NO excited electronic states. Secondly, the present model does not capture the complex dynamics of  $N_2(C^3\Pi_u)$ . It underestimates the rapid destruction of  $N_2(C^3\Pi_u)$  and does not predict its production after 50 cm. This may be due to processes not being taken into account in the new kinetic model.

## VI. References

- [1] Johnston CO, Brandis AM. Features of Afterbody Radiative Heating for Earth Entry. *J Spacecr Rockets* 2015;52:105–19. <https://doi.org/10.2514/1.A33084>.
- [2] Gessman R, Laux C, Kruger C, Gessman R, Laux C, Kruger C. Experimental study of kinetic mechanisms of recombining atmospheric pressure air plasmas. 28th Plasmadynamics Lasers Conf., Reston, Virginia: American Institute of Aeronautics and Astronautics; 1997. <https://doi.org/10.2514/6.1997-2364>.
- [3] Gessman RJ. An Experimental Investigation of the Effects of Chemical and Ionizational Equilibrium in

- Recombining Atmospheric Pressure Air Plasmas., Ph.D. Thesis, Stanford University, 2000.
- [4] Tibere-inglesse A. Radiation of nonequilibrium recombining plasma flows. Ph.D. Thesis, CentraleSupélec, Université Paris-Saclay, 2020.
- [5] Owano TG. Nonequilibrium behavior in a flowing, atmospheric pressure plasma. Ph.D. Thesis, Stanford University, 1991.
- [6] Grimaldi C, McGuire S, Laux CO. Temperature and radiation measurements of an atmospheric pressure CO<sub>2</sub> plasma. AIAA Scitech 2020 Forum, Reston, Virginia: American Institute of Aeronautics and Astronautics; 2020, p. 1–9. <https://doi.org/10.2514/6.2020-1708>.
- [7] Dubuet U, Mariotto P, Perrin M, Laux CO. Electronic-Specific Modeling of Nitric Oxide in a Recombining Air Plasma. AIAA Scitech 2021 Forum, Reston, Virginia: American Institute of Aeronautics and Astronautics; 2021, p. 1–23. <https://doi.org/10.2514/6.2021-0445>.
- [8] Laux CO, Pierrot L, Gessman RJ. State-to-state modeling of a recombining nitrogen plasma experiment. Chem Phys 2012;398:46–55. <https://doi.org/10.1016/j.chemphys.2011.10.028>.
- [9] Mariotto P. Study of nonequilibrium radiation in a N<sub>2</sub>/Ar recombining plasma flow. Ph.D. Thesis, CentraleSupélec, Université Paris-Saclay, 2022 (*to be published*).
- [10] Pierrot LC. Chemical kinetics and vibrationally-specific collisional radiative models for nonequilibrium nitrogen plasmas. Final Report of ESA Post-Doctoral Fellowship, 1999.
- [11] Popov NA. Kinetics of plasma-assisted combustion: effect of non-equilibrium excitation on the ignition and oxidation of combustible mixtures. Plasma Sources Sci Technol 2016;25. <https://doi.org/10.1088/0963-0252/25/4/043002>.
- [12] Capitelli M, Ferreira CM, Gordiets BF, Osipov AI. Plasma Kinetics in Atmospheric Gases. Plasma Phys Control Fusion 2001;43:371–2. <https://doi.org/10.1088/0741-3335/43/3/702>.
- [13] Minesi N. Thermal spark formation and plasma-assisted combustion by nanosecond repetitive discharges. Ph.D. Thesis, CentraleSupélec, Université Paris-Saclay, 2020.
- [14] Shkurenkov I, Burnette D, Lempert WR, Adamovich I V. Kinetics of excited states and radicals in a nanosecond pulse discharge and afterglow in nitrogen and air. Plasma Sources Sci Technol 2014;23. <https://doi.org/10.1088/0963-0252/23/6/065003>.
- [15] Rusterholtz DL, Lacoste DA, Stancu GD, Pai DZ, Laux CO. Ultrafast heating and oxygen dissociation in atmospheric pressure air by nanosecond repetitively pulsed discharges. J Phys D Appl Phys 2013;46. <https://doi.org/10.1088/0022-3727/46/46/464010>.
- [16] Laux CO. Optical Diagnostics and Radiative Emission of Air Plasmas. Ph.D. Thesis, Stanford University, 1993.
- [17] McBride BJ, Gordon S. Chemical Equilibrium with Applications 1992.
- [18] Guerra V, Sá PA, Loureiro J. Nitrogen pink afterglow: The mystery continues. J Phys Conf Ser 2007;63. <https://doi.org/10.1088/1742-6596/63/1/012007>.